ELSEVIER

3D high-resolution acoustic imaging of the sub-seabed

Martin Gutowski [a,b,*], Jonathan M. Bull [a], Justin K. Dix [a],
Timothy J. Henstock [a], Peter Hogarth [b], Tom Hiller [b],
Timothy G. Leighton [c], Paul R. White [c]

[a] *School of Ocean and Earth Sciences, National Oceanography Centre, Southampton, European Way,
Southampton SO14 3ZH, United Kingdom*
[b] *GeoAcoustics Ltd., Shuttleworth Close, Gapton Hall Industrial Estate, Great Yarmouth,
Norfolk NR31 0NQ, United Kingdom*
[c] *Institute of Sound and Vibration Research, Southampton University, Highfield,
Southampton SO17 1BJ, United Kingdom*

Abstract

Chirp sub-bottom profilers are marine acoustic devices that use a known and repeatable frequency-modulated source signature to produce vertical seismic reflection cross-sections of the sub-seabed. Here a 3D Chirp system is described that operates in the frequency range of 1.5–13 kHz, to produce a three-dimensional image of the sub-seabed, with typical penetration of 10–30 m and decimetric horizontal and vertical resolution. The system design incorporates a rigid frame that contains the Chirp source array together with 60 receiver elements, with positioning provided by an integrated real-time-kinematic (RTK) global positioning system (GPS). The system can be surface towed from a small survey vessel and can be applied to targets of marine geological, engineering, archaeological and defence interest. Data acquisition and processing are described for a case study which images a buried engineering structure in the Port of Southampton.
© 2006 Elsevier Ltd. All rights reserved.

Keywords: Chirp; 3D Chirp; 3D seismics; High-resolution seismics

* Corresponding author. Address: School of Ocean and Earth Sciences, National Oceanography Centre, Southampton, European Way, Southampton SO14 3ZH, United Kingdom. Tel.: +49 2183 416860.
    E-mail address: mxg@noc.soton.ac.uk (M. Gutowski).

1. Introduction

Seismic reflection methods use controlled acoustic sources to image the sub-surface. The hydrocarbon exploration industry has routinely used marine 3D seismic reflection methods for over 30 years to image geological structures down to kilometres depth, with vertical and horizontal resolutions of some tens of metres. However, near-surface, high-resolution, sub-bottom profiling typically still relies on single-channel 2D methods, the data from which have to be interpolated to give a pseudo-3D interpretation of buried structures. Consequently, the effective horizontal resolution of these data is controlled by the survey line spacing, which can be anything from a few metres to several hundred metres.

In contrast to the 2D method, the 3D method produces data volumes that can be processed coherently across a site. These processed volumes can then be visualised and interpreted to reveal the true three-dimensional geometry of the sub-surface with a horizontal resolution orders of magnitude better than 2D data, thus making it possible to detect small objects and reveal complex geometries. Further, by taking the three-dimensional wave propagation into account during data processing, 3D seismic reflection data can be of significantly higher quality.

There have been various attempts over recent years to downscale the 3D seismic reflection method to produce marine high-resolution 3D seismic data volumes by using high-frequency sub-bottom profiler sources. Henriet et al. [1] and Versteeg et al. [2] used boomer and water-gun sources with a frequency range of 1–5 kHz and 100–600 Hz, respectively; Marsset et al. [3], Missian et al. [4] and Missian [5] used a boomer source with a frequency range of 100–600 Hz; and Scheidhauer et al. [6,7] used a mini-airgun source with a frequency range of 50–650 Hz. Conventional 3D seismic systems typically use frequencies of tens of Hz, and consequently use receiver spacing of some metres and sampling rates of some hundred Hz. Higher sampling rates are needed to store the reflection data for the 1.5–13 kHz acoustic source signal used in this paper. In particular it is important that the receiver spacing is adapted to the frequency range to avoid spatial aliasing of the data, and to record adequately the absolute positions of the source and receiver elements during data acquisition. The design concept used in the 3D Chirp profiler described here, is to place all source and receiver elements on a rigid frame that is positioned using real time kinematic (RTK) GPS technology [8]. This is in contrast to the 3D high-resolution systems referenced above, which use lower frequencies and rely on individually towed and positioned source and receiver elements whose locations are monitored with conventional DGPS positioning.

This paper describes the design of the system, and the techniques used for data acquisition, processing and visualisation. Its capabilities are then illustrated using an engineering case study in the Port of Southampton, UK in which a buried object is located and imaged. The object, a coffer-dam, was deployed for geotechnical investigations associated with the building of the quay walls of the Prince Charles Container Terminal. On completion of these investigations it was toppled, *in situ*, into a pre-formed trench and buried. The coffer dam was constructed from steel sheets with wooden re-enforcements, with a square cross-section (4.6 m × 4.6 m) and a length of 16.5 m. An approximate position of one corner of the damn was available prior to the survey, which enabled the production of a survey grid 200 m × 25 m centred on this known point.

2. The 3D Chirp system

The 3D Chirp system, shown in Fig. 1, consists of a surface towed array made up of 11 2 m longitudinal sections. Altogether these sections hold a total of 60 receiver groups at 25 cm nodal spacing. The acoustic source consists of four Chirp transducers in a Maltese Cross configuration, positioned on buoyancy panels in the centre of the array and operating within a frequency range of 1.5–13 kHz. The array itself is constructed from glass-reinforced plastic and PVC foam, making it a rugged, lightweight and overall neutrally buoyant. The array is positioned using RTK-GPS positioning technology together with a GPS based attitude (heading, pitch and roll) system. The four GPS antennas are placed at the corners of the array on staves 0.9 m in length, which ensure that they stay above the water surface during deployment. The structure of the array was designed to achieve stable
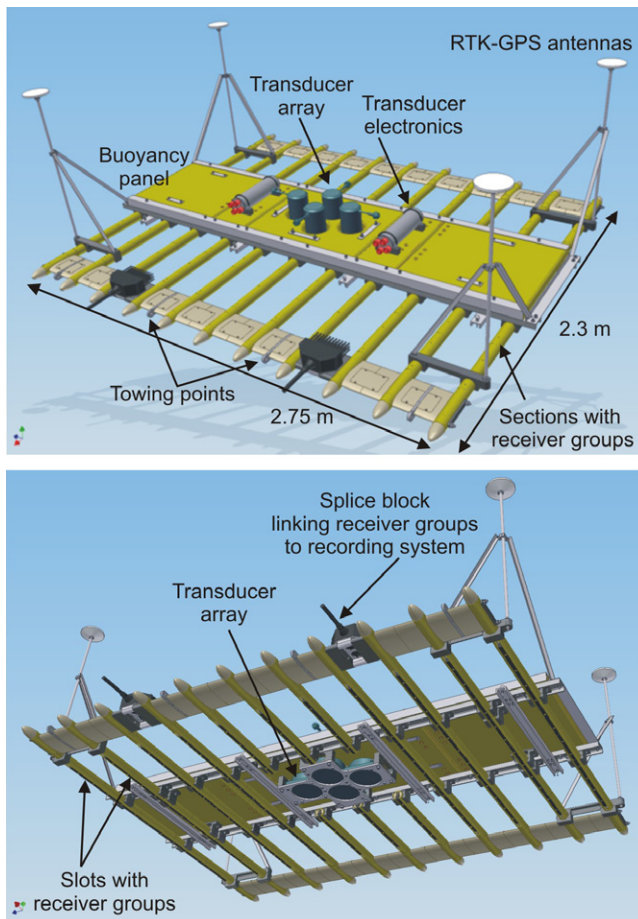

Fig. 1. 3D Chirp high-resolution sub-bottom profiling system. The surface towed rigid 2.75 m wide by 2.3 m long frame holds 60 receiver groups in the longitudinal sections and a four-transducer source array on a central buoyancy panel. The transducers operate at a bandwidth of 1.5–13 kHz. It is positioned using RTK-GPS and an attitude systems with four GPS antennas attached to the frame.

towing behaviour with minimal drag to reduce hydrodynamic noise generation. It is not only ideal for small vessel deployment in coastal waters, rivers and lakes, but also for transportation of the system by small aircraft from its home base to remote locations around the world. The construction concept makes it easy to expand the array as required by adding sections with additional receiver groups.

Fig. 2a shows the system deployed on the 12 m long R/V Bill Conway and Fig. 2b shows the system being towed. The seismic data is recorded with a custom-built seismograph that allows the simultaneous recording of 60 channels, with a maximum sampling frequency of 50 kHz at 16-bit resolution. The system uses a network time protocol (NTP) server to ensure accurate GPS time stamping of the seismic and navigation data, thus facilitating their merger during the processing phase.

2.1. Source signatures

Chirp sources are marine wide-band, frequency-modulated, sub-bottom profilers that produce high-quality, high-resolution seismic reflection data. They comprise calibrated, linear electronics that are capable of producing a highly repeatable source signature [9,10]. They transmit a frequency modulated (FM) signal that is corrected for the source and receiver phase and amplitude responses. Owing to the wide bandwidth of the signal, optimum penetration, as well as resolution, can be achieved. The signal-to-noise-ratio (SNR) is improved through matched filter processing by correlating the reflection data with the transmitted pulse. Gutowski et al. [11] discuss different source signatures to be used with the 3D Chirp system for optimal resolution and penetration. Fig. 3 shows the source signature used for the data-set discussed in this paper, which is widely used in the commercial Chirp system and uses a Blackmann–Harris envelope function [12] and a linear instantaneous frequency function, over a frequency range of 2–8 kHz.

2.2. Acquisition geometry

In designing the system a balance had to be achieved between the competing needs of (1) ensuring that there was no spatial aliasing; (2) that the total number of recorded chan-
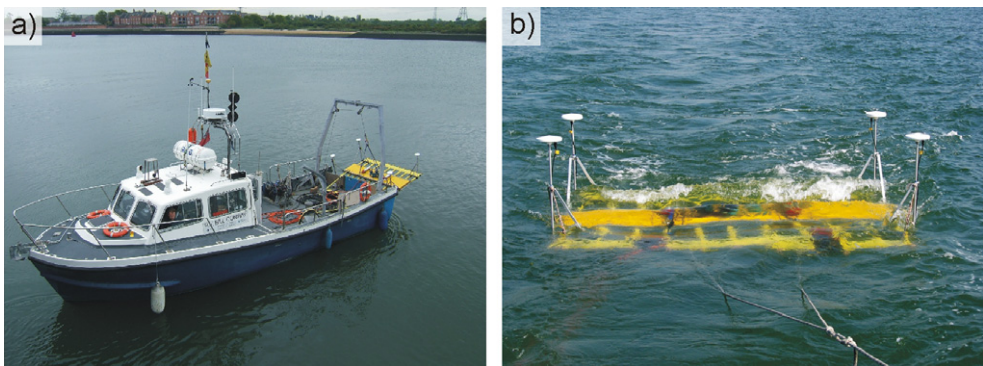

Fig. 2. (a) The 3D Chirp system is deployed from the A-frame of the 12 m long R/V Bill Conway. (b) Its lightweight open and rugged construction results in neutral buoyancy and assures a stable towing behaviour. The GPS antennas stay above the sea surface during the survey.
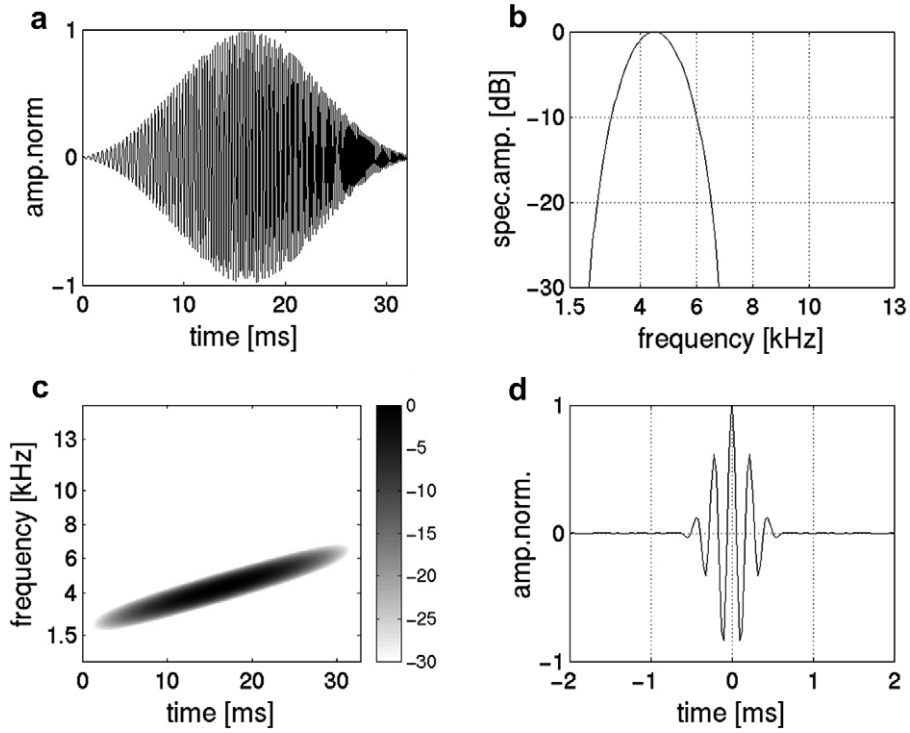
Fig. 3. Linear low frequency Chirp source sweep with Blackmann–Harris envelope function. (a) Time domain representation. (b) Power spectrum with a mean frequency of 4.5 kHz. (c) Spectrogram showing the linear instantaneous frequency function. The greyscale represents the same dB scale as in the spectrum. (d) Klauder wavelet, the normalised auto-correlation function of the sweep.

nels was manageable; (3) that a 3D volume could be obtained under normal surveying conditions. Particular consideration was given to ensuring that spatial aliasing of the data is avoided (e.g., [13]). In the spatial domain, apparent wavelengths, smaller than twice the spacing of the receiver elements, are spatially aliased. This has implications for wavefield based data processing stages, such as the pre-stack Kirchhoff migration described in this paper. With a receiver spacing Δx_{rec} in the array, and energy with wavelength λ incident on the array at angle α from the vertical, this requires that

$$\Delta x_{rec} < \frac{\lambda}{2 \sin \alpha}.$$

The receiver spacing required for this is smaller for shorter wavelengths or for incident energy that travels at an angle close to the horizontal. Clearly there is an additional factor that for a fixed number of channels, the smaller the receiver spacing used, the smaller the overall footprint of the array will be, and the more closely spaced must be individual survey-lines to assure the full coverage of the survey area. Hence for efficiency Δx_{rec} must be maximized while minimizing potential problems of spatial aliasing. The most likely origin for problematic aliased energy is by scattering at the seabed because, for a given recording time, the energy will travel at the shallowest angles and have the highest ampli-

tudes. Hence the effect of such scattered energy, including the directivities of each element in the hardware, has been modelled and the receiver spacing of 25 cm was found to be the optimum (see [8] for further details).

2.3. Positioning

The accuracy required for the positioning of the source and receiver elements of the 3 D Chirp system depends on the characteristics of the source signature used. The required accuracy in the vertical direction results from the necessity to stack seismic traces in a common mid-point bin defined in the geometry assignment during the 3D data processing, i.e. adding data traces which have been recorded within a minimum bin size of 12.5 cm × 12.5 cm. The bin size represents the distances between two reflection points recorded with a receiver spacing of 25 cm. In order to avoid destructive interference when stacking the seismic traces, the error in its associated vertical positions need to be smaller then the distance between the main-lobe peak and the side-lobe trough of the signature's Klauder wavelet (Fig. 3). The time-difference between the lobes is 105 μs for the sweep used in the survey detailed in this paper [8,11], which is equivalent to a required vertical accuracy of ±8 cm assuming a compressional p-wave velocity of 1500 m s^{-1} in water.

In order to reconstruct the wavefield adequately, the horizontal position needs to be known within a quarter of the wavelength, $\lambda/4$. For the Klauder wavelet of this pulse, which has a dominant frequency of 4.66 kHz, this is equivalent to ±4 cm (assuming a p-wave velocity of 1500 ms^{-1} in water). Furthermore, the positions need to be measured reliably with an update rate similar to the seismic shot rate (between 4 and 8 shots per second). The solution used to address these constraints with the absolute accuracy required to acquire true 3D data was to place the source and receiver elements on a plane and rigid array, so that the source–receiver offsets are known *a priori*. The array can then be positioned using in this case a Thales Sagitta RTK GPS and a Thales ADU5 attitude system. Static tests on this navigation set-up gave horizontal and vertical accuracies of the absolute position of the source and receiver element positions of ±0.7 cm and ±1.82 cm, respectively, both within the theoretical constraints.

3. Data acquisition and processing

Fig. 4 shows the diagram representing the flow used to process the 3D Chirp data. During the initial geometry processing stage the source and receiver positions are assigned to the relevant trace of the seismic data. The rigid frame of the 3D Chirp system allowed the geometry to be calculated by solid body rotation calculation. Firstly the time-stamped RTK-GPS positions and GPS attitude files are interpolated on the shot events from the seismic acquisition files. Secondly the source and receiver positions are calculated for each channel using their relative positions on the array, together with the interpolated navigational data. Lastly, the information is written into the trace headers of the seismic data for subsequent processing.

After the geometry processing, the data are band-pass filtered using an Ormsby zero phase frequency domain filter with Hanning taper functions. It is set such that the source signal bandwidth is conserved. The data are then correlated with the source sweep shown in Fig. 3. The resulting traces now represent the convolution of the Klauder wavelet of the source signature with the sub-surface's impulse response function (plus noise). The instan-
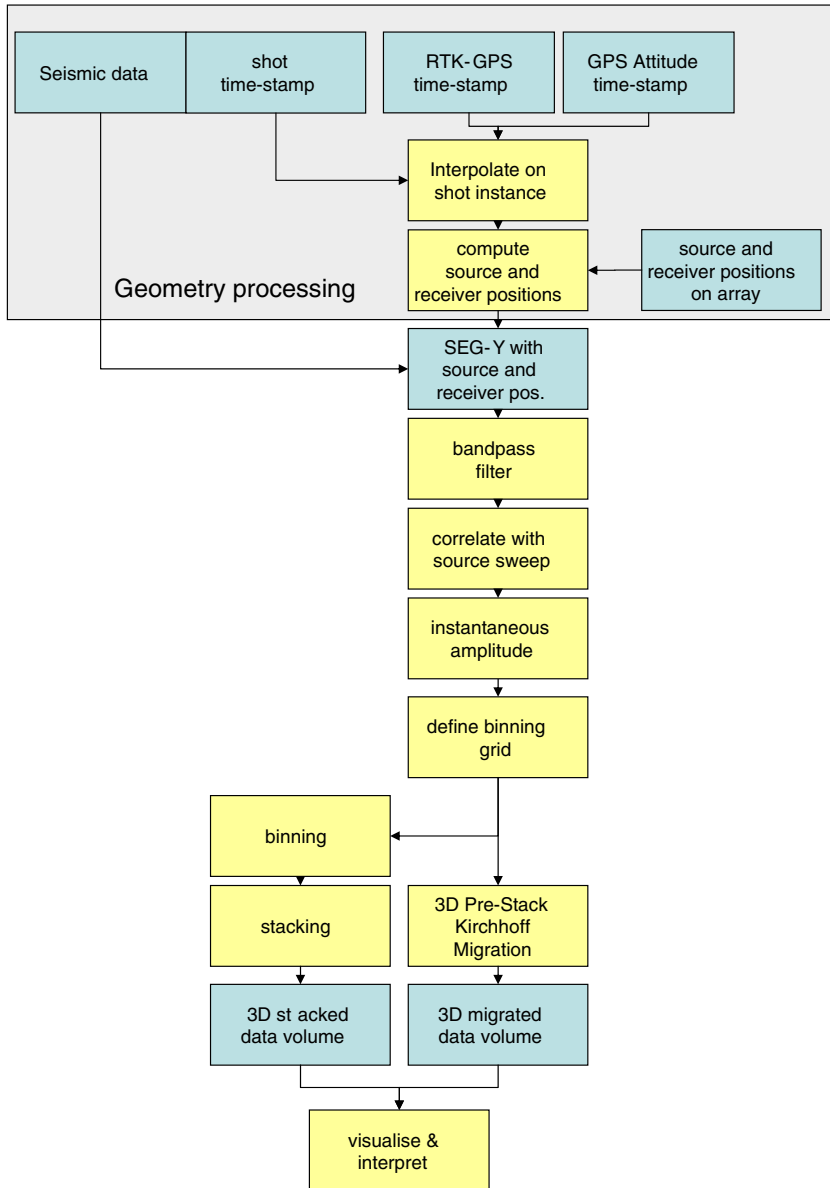
Fig. 4. Data processing flow. See text for details.

taneous amplitude, the envelope function of the data, is then typically computed. This is a standard processing step for Chirp data and improves its interpretability [14].

The next step is to define a binning grid to cover the survey area (Fig. 5); in this paper each bin size is 12.5 cm × 12.5 cm square. Subsequently there are two options for further processing. The first option is to bin the data on the defined grid. The data are then stacked and the mean values of the trace samples within each bin are calculated. This
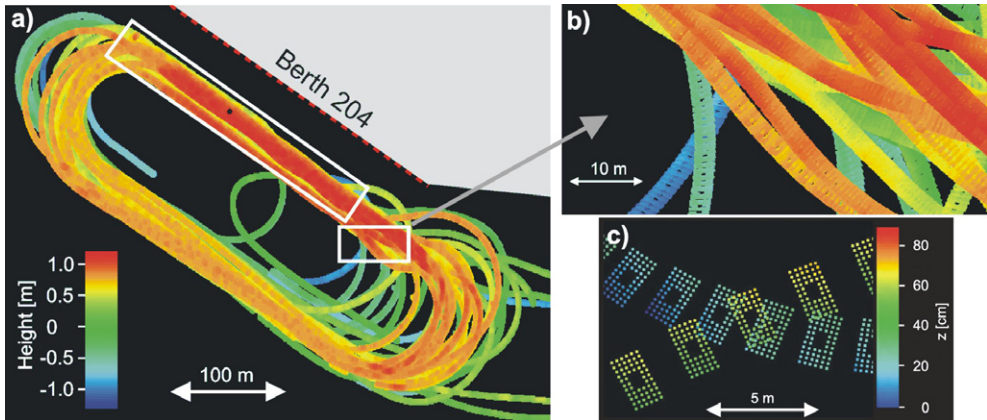
Fig. 5. (a) Position of receiver elements during the survey marking the track of the source array during data collection along the quay wall of Berth 204 in the Port of Southampton where a coffer-dam is buried beneath the seabed. The area of interest is highlighted together with an area shown as a close-up in (b). The colours represent the deviation of the receiver heights from their average. The height differences of approximately 2.3 m are due to the differences of tidal heights present during the 6 h survey period. (b) The close-up highlights the individual survey lines made up of squares marking the positions of the individual receiver groups at a shot-instant. (c) A further close-up shows the positions of receiver elements for every fourth shot only, highlighting receiver positions for individual shots. Two individual survey lines are apparent and the receiver heights variation is visible on the colour scale for this figure. The array tilts during towing through a bend, which is reflected in the receiver height difference of up to 25 cm for receivers on opposite corners of the array (for interpretation of color in this figure, the reader is referred to the web version of this article).

results in an improvement of the signal to noise ratio [13]. The stacked volume can then be loaded into software for 3D seismic interpretation.

Alternatively the data can be migrated using a 3D pre-stack Kirchhoff migration algorithm. Migration moves recorded seismic reflection energy to its true position in the time/space domain. In particular it moves dipping reflectors into their true positions, increasing their dip, and collapses diffraction hyperbolas, thereby delineating sub-surface features. As a result it increases spatial resolution, up to the mean wavelength of the source signatures used [13]. The algorithm used here is based on the Kirchhoff migration, which carries out summations of amplitudes along hyperbolic paths. The summation is assigned to the hyperbola apexes, which are considered as point diffractors generating the diffraction hyperbolas. Imaged reflection interfaces are produced by superposition of diffraction points. The amplitudes are corrected for the effects of spherical spreading, the obliquity factor (angular dependency of amplitudes) and phase shifts. The seismic velocity of the sub-surface governs the curvature of the hyperbola. See for example Schneider [15] for formulation of the Kirchhoff algorithm for 2D and 3D data. In the case of 3D migration, the summation is performed over the surface of a hyperboloid and assigned to its apex after applying the aforementioned corrections. For the pre-stack migration algorithm used here, the source receiver offsets are taken into account and the amplitudes are summed along travel time trajectories that depend on velocity structure and acquisition geometry, or travel time surfaces for the 3D case. The practical advantage, and the reason this migration algorithm was chosen over other available algorithms, is that it deals with erratic distribution of source and receiver positions as is the case in the 3D Chirp dataset. A constant

migration velocity of 1500 m s^{-1} is used as a more complex velocity model from the 3D data set was not extracted, since a velocity analysis is not feasible with the given source–receiver offsets smaller than 2 m in the given water-depth [13]. The algorithm uses a 4 m migration aperture (defined as the radius of a circle centred at the imaging trace providing the area from which traces are considered for the migration).

Fig. 5 shows the positions of the receiver elements for seismic shots during the survey (receiver positions in the SEG-Y data in Fig. 4). Fig. 5a reveals the extent of the survey,
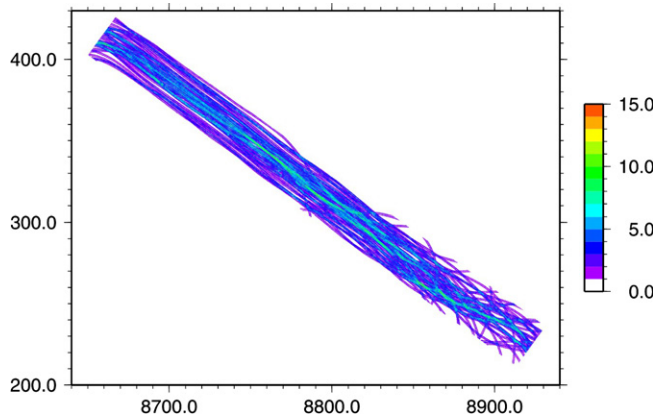

Fig. 6. Data coverage. The colour scale represents the cdp-fold, which is the number of reflection points, i.e. the mid-point between source and receiver element, in 12.5 cm × 12.5 cm bins within the grid (outline highlighted in Fig. 5a). The cdp-fold ranges from 0 which represents data gaps to 15 for isolated cases (for interpretation of color in this figure, the reader is referred to the web version of this article).
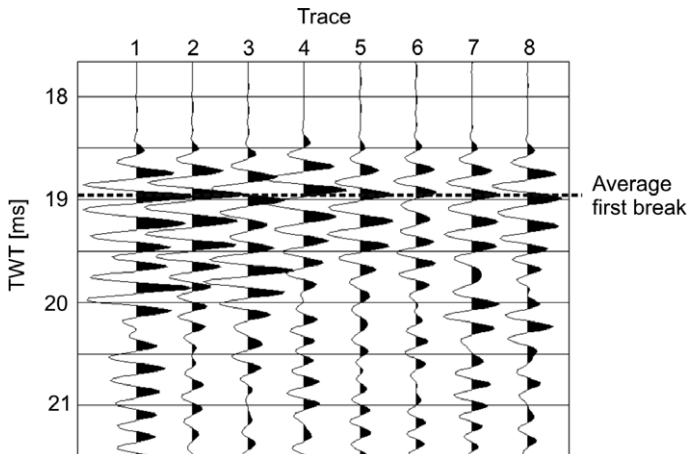

Fig. 7. Figure demonstrating consistency of data and reliability of navigation within a single bin. Individual traces within a single bin (of size 12.5 cm × 12.5 cm) recorded during five separate survey line passes over the same area over a period of 3.5 h with a corrected tidal height difference of up to 1.7 m. The average seabed reflection time is 18.98 ms (c. 14.24 m) with a standard deviation of 0.03 ms (c. 2.4 cm).

which was conducted by sailing lines parallel to the Berth 204 quay wall in the Port of Southampton. The white square outlines the binning grid. The height is plotted as deviation from the mean value; note that there is a variation of approximately 2.3 m, which is due to the changes in tidal heights during the survey time of 6 h. If the data is more closely inspected (Fig. 5b), the individual squares, comprising 60 receiver group positions representing individual shots, become apparent. In a further close-up, Fig. 5c shows receiver positions for every fourth shot on two crossing survey lines. With the vertical scale in Fig. 5c representing a height range of only 83 cm, receiver height differences of up to 25 cm between receivers on opposite corners are captured in the data as the array is tilted during a turn.

Fig. 6 illustrates the binning grid with the number of traces within each 12.5 cm square bin denoted by the colour scale. It ranges from 0 (data gaps) to 15 in some isolated cases and represents the data fold in the survey area. The data gaps are largely filled by the interpolating effect of the migration algorithm.

Earlier it was established that the vertical positioning needs to be better than ±8 cm to ensure good data improvements on stacking traces within a bin. One check of navigation
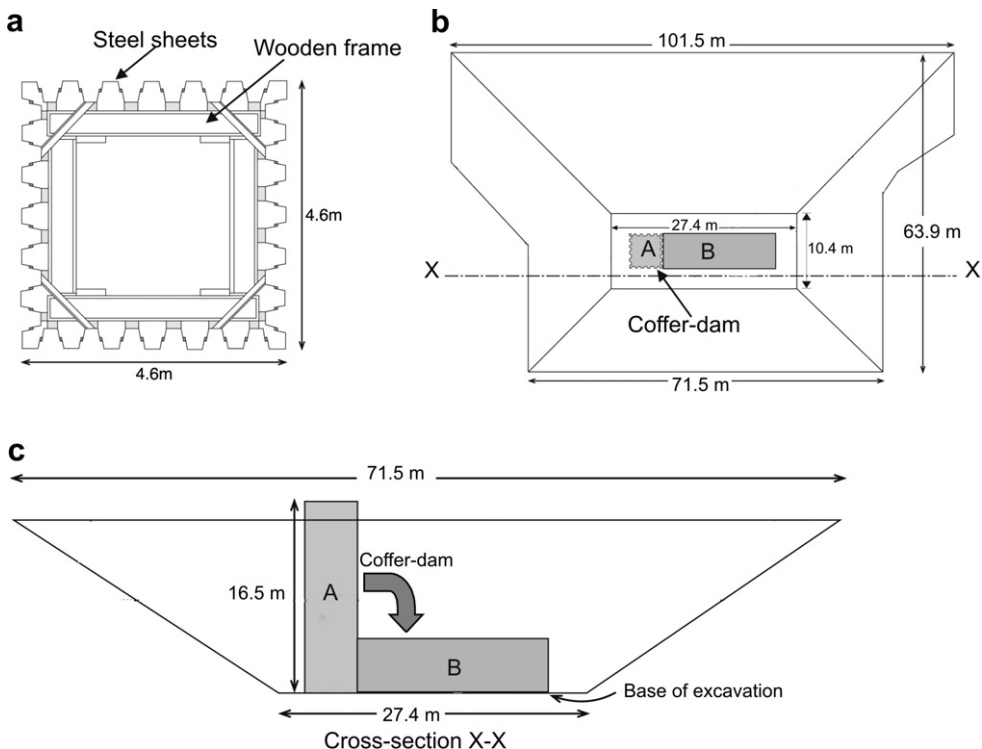

Fig. 8. Engineering drawings of the coffer-dam and the excavated trench. (a) The square cross-section of the coffer-dam with a side-length of 4.6 m. It was constructed from steel sheets which are reinforced with a wooden frame. (b) A map view of the excavated trench with the coffer-dam in both its original upright position (A) and expected toppled position (B) (c) cross-section X–X highlighted in (b) with the coffer-dam in its original upright position (A) with a height of approximately 16.5 m and toppled position (B). The coffer-dam was buried with sediment after toppling into a semi-horizontal position on the trench base.

quality is to look at consistency of the seabed arrival within a single representative bin. Fig. 7 shows eight traces within a single bin collected during five survey-line passes over the same area in a period of 3.5 h with a corrected tidal height difference of up to 1.7 m. The average first break (the return from the seafloor) is highlighted. The standard deviation of the first break in this bin is ±0.03 ms TWT (two way time), which represents a distance of ±2.25 cm (assuming a constant p-wave velocity in water of 1500 m s^{-1}), clearly illustrating that the dynamic vertical positioning accuracy is well within the theoretically derived limits.

4. The data volume

During the construction of the Prince Charles Container Terminal in the Port of Southampton, an engineering investigation of the stability of the seabed was undertaken using a coffer-dam, which was driven into the ground close to the construction site. The coffer-dam comprised steel sheet-piles reinforced with a wooden frame (Fig. 8a). After completion of the testing, a trench was excavated around the structure, into which the coffer-dam was toppled and subsequently buried. Engineering drawings of the trench in both plan-view (Fig. 8b) and cross-section (Fig. 8c) show the inferred relative position of the coffer-dam before and after toppling. The existence of these engineering drawings make the coffer-dam and associated trench an excellent target to test the capabilities of the 3D Chirp system.

The migrated data volume, shown in Fig. 9, covers an area of 200 m × 25 m, centred on the coffer-dam and the deepest part of the excavated trench. Sections of the data can be viewed in any orientation, independent of the original survey direction. Vertical slices in the direction of the longer side of the rectangular survey area, called inlines, and vertical section perpendicular to these, called crosslines are highlighted together with a horizontal timeslice, representing the reflection amplitudes at a constant TWT. The seafloor is at
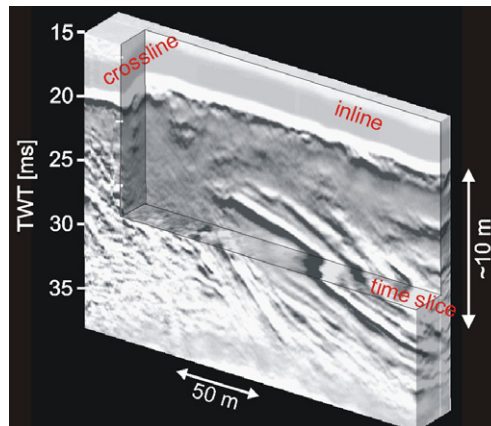

Fig. 9. 3D Chirp data volume over the coffer-dam area. The data volume is 200 m long × 25 m wide area and images structures down to 15 m below the seafloor. Note the vertical inline and crossline sections together with the horizontal timeslice. Dipping bedrock reflectors are apparent which are overlain by soft sediments and interrupted by a trench containing the buried coffer-dam. Note that a pre-stack 3D Kirchhoff migration has been applied.

20 ms TWT which equals approximately 15 m water-depth and the sub-surface penetration is also approximately 15 m.

Representative vertical cross-sections (inlines – Fig. 10) and horizontal slices (time slices – Fig. 11) clearly show the outline of the coffer-dam and the excavated trench. The inline displayed in Fig. 10c crosses through the expected centre of the trench base and over the expected position of the coffer-dam as defined by the engineering drawings (Fig. 8). The inline displays a reflection at c. Twenty milliseconds TWT which corresponds to the seabed, under which is 2–3 ms TWT of transparent material, which is interpreted to be a veneer of soft sediments (confirmed by direct grab sampling). Away from the expected position of the trench, dipping reflectors (dip angles between 5° and 11°) are imaged which are interpreted to be bedrock. A disturbed zone of reflectors corresponds to the position of the trench, and within this zone a high amplitude reflection, approximately 2 ms TWT
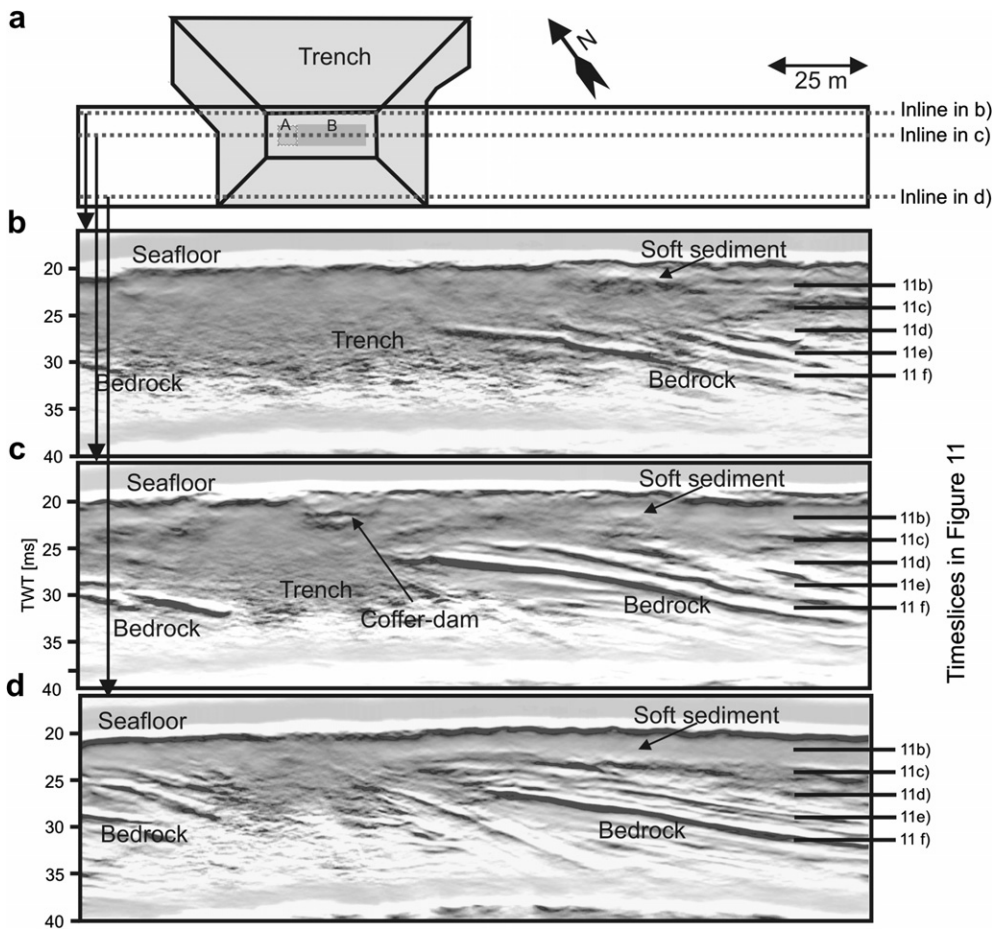

Fig. 10. (a) Spatial extent of the data volume (Fig. 9) over the excavated trench and coffer-dam. The coffer-dam is shown in its original construction position (A) and after toppling (B) onto the trench base where it was subsequently buried. The positions of the inline sections shown in (b)–(d) are marked. The locations of the timeslices which are shown in Fig. 11 are also indicated. See text for more details.

below the seafloor is apparent. This reflector is interpreted as the top of the buried coffer-dam, and is consistent with the expected position after toppling of the original structure within the trench. The length of the reflector, approximately 14 m, is similar to the approximate height of the coffer-dam of 16.5 m (Fig. 8) giving support to the interpretation.

Fig. 10b shows an inline towards the north-eastern extremity of the trench base, where the engineering drawing indicated that the trench had broader flanks (Fig. 10a). The disturbed zone is wider and the reflection event associated with the coffer-dam is not present. Fig. 10d shows an inline towards the south western edge of the trench. As predicted there is little evidence for the trench, and the bedrock reflections are continuous up to 2–3 ms TWT beneath the seabed.

The positions of the time slices shown in Fig. 11 are marked in the inline sections in Fig. 10. Fig. 11a shows the area covered by the data volume overlain by the map of the trench with the position of the coffer-dam before and after toppling. Fig. 11b shows the timeslice at the depth of the coffer-dam at 21.7 ms TWT. A strong reflection with two linear edges, is found at a position that correlates with the expected position of the coffer-dam within the trench. The clear imaging of only two edges suggests that the coffer-
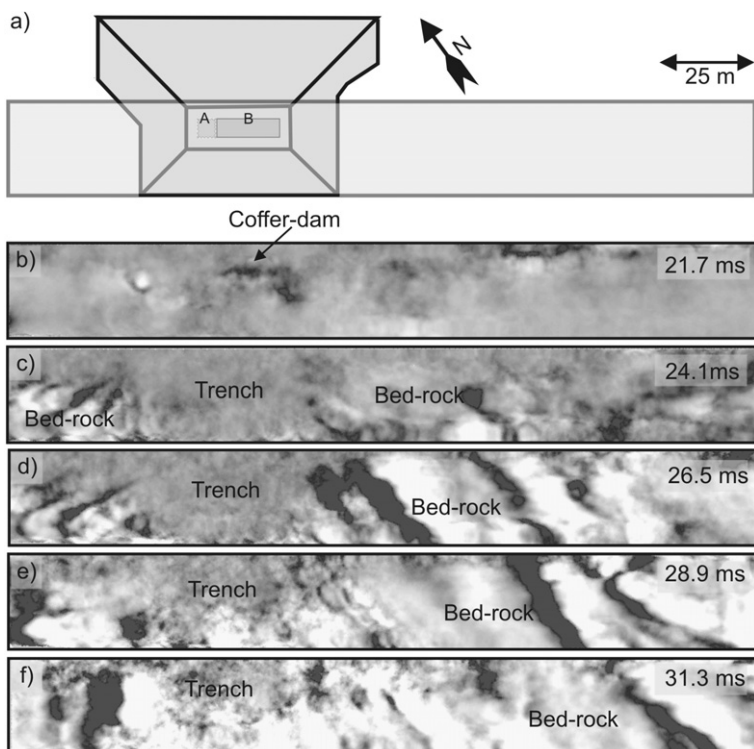

Fig. 11. (a) Spatial extent of the data volume (Fig. 9) over the excavated trench and coffer-dam. The coffer-dam is shown in its original construction position (A) and after toppling (B) onto the trench base where it was subsequently buried. (b) Timeslice at 21.7 ms TWT (c. 16.3 m depth) imaging the horizontal outline of the coffer-dam. (c) Timeslice at 24.1 ms TWT (c. 18.1 m depth) showing the horizontal extent of the trench matching the map in (a) which is bordered by linear bed-rock reflection to either side. (d) Timeslice at 26.5 ms TWT (c. 19.9 m depth). (e) Timeslice at 28.9 ms TWT (c. 21.7 m depth). (f) Timeslice at 31.3 ms TWT (c. 23.5 m depth).

dam is gently inclined to the south-west. Figs. 11c–f show timeslices in regular intervals of 2.4 ms TWT (c. 1.8 m) below the first timeslice. The outlined homogeneous zone interpreted as the trench agrees with the engineering drawing shown in Fig. 11a. Linear features on either side of the trench are associated with reflections from the dipping bedrock layers.

5. Conclusions

The 3D Chirp system provides the capability of true 3D imaging of the top c. 20 m of the sub-seabed with decimetric resolution in x, y and z. The capability of the system was demonstrated in a case study in which a buried object within the Port of Southampton was successfully imaged. The capability of the 3D Chirp system to image complex geometries and small objects in the sub-surface with high resolution makes it a valuable tool for marine engineering, defence, marine archaeology as well as general marine geology and geophysics applications. As well as the data example discussed here, the system has been successfully applied to image buried shipwrecks and locate small objects buried in a harbour basin.

Acknowledgements

Appendix A. Supplementary data

Supplementary data associated with this article can be found, in the online version, at doi:10.1016/j.apacoust.2006.08.010.

References

[1] Henriet JP, Verschuren M, Versteeg W. Very high resolution 3D seismic reflection imaging of small-scale structural deformation. First Break 1992;10:81–8.
[2] Verstegg W, Verschuren M, Henriet J-P, De Batist M. High resolution 3D and pseudo-3D seismic investigations in shallow water environments. In: Weydert M, editor. European conference on underwater acoustics. London: Elsevier Applied Science; 1992. p. 497–500.
[3] Marsset B, Missiaen T, De Roeck Y-H, Noble M, Versteeg W, Henriet J-P. Very high resolution 3D marine seismic data processing for geotechnical applications. Geophys Prospect 1998;46:105–20.
[4] Missiaen T, Versteeg W, Henriet J-P. A new 3D seismic acquisition system for very high resolution and ultra high resolution shallow water studies. First Break 2002;20:227–32.
[5] Missian T. VHR marine 3D seismics for shallow water investigations: some practical guidelines. Mar Geophys Res 2005;26:145–55.
[6] Scheidhauer M, Dupuy D, Beres M, Marillier F. Development of a 3D VHR seismic reflection system for lacustrine settings – a case study in Lake Geneva, Switzerland. EGS-AGU-EUG Joint Assembly, Nice, France, 6–11 April 2003, Abstract EAE03-A-02720.
[7] Scheidhauer M, Dupuy D, Beres M, Marillier F. Development of a system for 3D high-resolution seismic reflection profiling on lakes. Mar Geophys Res 2005;26:183–95.

 [8] Bull JM, Gutowski M, Dix JK, Henstock TJ, Hogarth P, Leighton TG, et al. Design of a 3D Chirp sub-bottom imaging system. Mar Geophys Res 2005;26:157–69.

 [9] Schock SG, LeBlanc LR. Chirp sonar: new technology for sub-bottom profiling. Sea Technol 1990;31(9):35–43.

[10] Bull JM, Quinn R, Dix JK. Reflection coefficient calculation from marine high-resolution seismic reflection (Chirp) data. Mar Geophys Res 1998;20:1–11.

[11] Gutowski M, Bull J, Henstock T, Hogarth P, Leighton T, White P. Chirp sub-bottom profiler source signature design. Mar Geophys Res 2002;23:481–92.

[12] Harris FJ. On the use of windows for harmonic analysis with discrete Fourier transform. Proc IEEE 1978;66:51–83.

[13] Yilmaz Ö. Seismic data processing. Investigations in geophysics, No. 2. Society of Exploration Geophysicists, Tulsa, Oklahoma, 1987.

[14] Quinn R, Bull JM, Dix JK. Optimal processing of marine high-resolution seismic reflection (Chirp) data. Mar Geophys Res 1997;20:13–20.

[15] Schneider W. Integral formulation for migration in two and three dimensions. Geophysics 1978;43:49–76.